Journal of Integrative Neuroscience

J. Integr. Neurosci. **2026**; 25(11): 55171
https://doi.org/10.31083/JIN55171

Original Research

Differential Neurophysiological Signatures of Asymptomatic Carotid and Intracranial Atherosclerotic Stenosis: A Multimodal Resting-State EEG Study

Pengcheng Zhao[1,2], Xueqian Song[3], Huanhuan Li[1,2], Henan Zhou[2], Keyuan Li[2,4], Zhezhi Liu[2,4], Jian Song[1,2,*], Guozheng Xu[1,2,*]

[1]The First School of Clinical Medicine, Southern Medical University, 510515 Guangzhou, Guangdong, China
[2]Department of Neurosurgery, General Hospital of Central Theater Command, 430070 Wuhan, Hubei, China
[3]Department of Cadre Ward First, General Hospital of Central Theater Command, 430070 Wuhan, Hubei, China
[4]Medical College, Wuhan University of Science and Technology, 430065 Wuhan, Hubei, China
*Correspondence: songjian0505@smu.edu.cn (Jian Song); xu-gz@163.com (Guozheng Xu)
Academic Editor: Imran Khan Niazi
Submitted: 22 June 2026 Revised: 28 July 2026 Accepted: 11 August 2026 Published: 18 November 2026

Abstract

Background: Chronic cerebral hypoperfusion associated with asymptomatic atherosclerotic cerebrovascular stenosis may induce functional-network alterations before overt neurological deficits emerge. Asymptomatic carotid stenosis (ACS) and asymptomatic intracranial atherosclerotic stenosis (aICAS) represent distinct large-artery phenotypes with differing perfusion distributions. However, whether these location-specific hemodynamic constraints are associated with different patterns of functional brain reorganization is poorly understood. This study investigated the multiscale electrophysiological alterations associated with ACS and aICAS. **Methods:** In this cross-sectional study, 68 participants, including ACS (n = 29), aICAS (n = 17), and age-matched healthy controls (n = 22), underwent resting-state electroencephalography (rs-EEG) recording and neuropsychological assessment (Chinese Mini-Mental Status [CMMS], Trail Making Test Parts A and B [TMT-A/B]). Microstate dynamics, power spectra, and α-band source-space functional connectivity were analyzed. Network-Based Statistic (NBS) controlled for family-wise error in connectivity analysis. Partial correlations adjusted for age, hypertension, and diabetes. Receiver operating characteristic (ROC) performance was evaluated using bootstrap confidence intervals and repeated five-fold cross-validation. **Results:** CMMS scores did not differ among groups, whereas TMT completion times were longer in the ACS group, indicating subtle performance alterations. Both patient groups showed reduced microstate A (MsA) coverage and decreased transitions between MsA and microstate C (MsC). ACS additionally exhibited shortened MsA duration, reduced α-band power, and increased connectivity within a distributed network identified by NBS. The aICAS group showed increased bidirectional transitions between microstate B (MsB) and microstate D (MsD) but no significant NBS component. Selected microstate measures remained associated with TMT performance after covariate adjustment. ROC analyses showed moderate discrimination, with apparent areas under the curves (AUCs) of 0.672–0.744 and cross-validated AUCs of 0.675–0.744. **Conclusions:** ACS and aICAS showed shared and location-specific electrophysiological alterations. These exploratory findings may help characterize early functional brain changes associated with asymptomatic cerebrovascular stenosis, but require confirmation in larger independent cohorts.

Keywords: carotid stenosis; intracranial arteriosclerosis; electroencephalography; cortical synchronization; cognition

1. Introduction

Atherosclerotic cerebrovascular stenosis compromises brain function via thromboembolism, hypoperfusion, and watershed infarction, forming the pathological core of ischemic stroke [1]. Before overt neurological deficits emerge, most patients pass through an extended asymptomatic phase that is frequently overlooked clinically. Asymptomatic carotid stenosis (ACS) and asymptomatic intracranial atherosclerotic stenosis (aICAS) are two major large-artery atherosclerosis phenotypes encountered during this period. Community-based cohort data placed moderate-to-severe ACS prevalence at roughly 7.5% [2], whereas moderate-to-severe aICAS affects 6–13% of the general population [3]. Despite the absence of focal neurological deficits, chronic cerebral hypoperfusion quietly drives white matter microstructural damage and reduced neural-network efficiency [4,5]. ACS and aICAS differ considerably in anatomical location, collateral compensation, and perfusion distribution, yet direct neurophysiological evidence comparing whether these differences produce divergent trajectories of brain functional change has not been established [6,7].

A key distinction between the two conditions relates to the chronicity of hemodynamic compromise. Unlike acute vascular occlusion, atherosclerotic stenosis unfolds gradually over months to years, giving the brain an extended window for neurovascular autoregulation and experience-dependent neuroplasticity [8]. The pathway from vascular stenosis to observable network change is not straight-

Copyright: © 2026 The Author(s). Published by IMR Press.
This is an open access article under the CC BY 4.0 license.

Publisher's Note: IMR Press stays neutral with regard to jurisdictional claims in published maps and institutional affiliations.

forward; it is mediated by the electrophysiological consequences of neuronal ischemia [9]. Chronic hypoperfusion progressively degrades membrane excitability, disrupts synaptic transmission, and alters large-scale oscillatory discharge patterns. Those intermediate neurophysiological changes, rather than the vascular lesion itself, drive network-level reorganization detectable by electroencephalography (EEG) [10]. Notably, vascular stenosis severity, electrophysiological network disruption, and cognitive decline constitute three partially dissociable axes of disease expression, and the degree of mismatch across these dimensions can provide information about individual variability in functional brain alterations [11].

Investigations into subclinical brain damage have drawn on neuropsychological assessments and neuroimaging. Neuropsychological tools, including the Mini-Mental State Examination, have been used to assess cognitive function and changes following revascularization in patients with carotid stenosis [12,13]. However, MMSE scores may be influenced by practice effects during repeated administration and by educational, cultural, and linguistic factors [14,15]. Neuropsychological assessments characterize behavioral performance but do not directly measure the associated neurophysiological alterations. Regarding neuroimaging, resting-state functional magnetic resonance imaging (rs-fMRI) studies have identified frequency-specific alterations in spontaneous activity within the default-mode network in severe ACS [16]. That said, rs-fMRI relies on hemodynamic responses as a proxy for neural activity, a dependency that becomes particularly problematic under chronic hypoperfusion and impaired neurovascular coupling, in which cases functional connectivity estimates may be systematically distorted [17].

Resting-state EEG (rs-EEG) directly records cortical electrophysiological oscillations at millisecond resolution, independent of cerebrovascular dynamics and blood-oxygen-level-dependent (BOLD) signal assumptions, making it better suited to capture intrinsic neural-network alterations under hypoperfusion [18]. Despite this advantage, previous EEG work has largely concentrated on symptomatic stenosis or isolated spectral abnormalities [19,20]. A framework integrating microstate dynamics, power spectral analysis, and source-space functional connectivity has not been developed, and a rigorous electrophysiological comparison of ACS and aICAS is conspicuously absent from the literature.

To address this gap, the present study enrolled ACS patients, aICAS patients, and healthy controls for comparative analysis of rs-EEG microstate dynamics, power spectra, and source-space functional connectivity, and to examine their relationships with neuropsychological assessment. The goal was to characterize the distinct neurophysiological profiles and heterogeneous patterns of brain reorganization associated with extracranial vs. intracranial atherosclerotic stenosis, and to provide preliminary electrophysiological evidence for characterizing brain functional alterations before stroke.

2. Materials and Methods

This cross-sectional observational study is reported in accordance with the Strengthening the Reporting of Observational Studies in Epidemiology (STROBE) guidelines. The completed STROBE checklist is provided as **Supplementary Material** (Supplementary STROBE Checklist).

2.1 Participants

Data collection was conducted at the General Hospital of the Central Theater Command from June 2024 to June 2025. An a priori sample size estimation was performed using G*Power 3.1 (Heinrich Heine University, Düsseldorf, Nordrhein-Westfalen, Germany), selecting the F-test family and "ANOVA: Fixed effects, omnibus, one-way". With three groups, an assumed allocation ratio of 1:1:1, an effect size of $f = 0.40$, $\alpha = 0.05$, power $1–\beta = 0.80$, the minimum balanced sample size was 66 participants (22 per group) [21]. A total of 68 participants were enrolled and allocated into three groups: the ACS group ($n = 29$), the aICAS group ($n = 17$), and the healthy control group (CG; $n = 22$).

Inclusion criteria for the ACS and aICAS groups were: (1) age 50–65 years with ≥6 years of formal education; (2) unilateral stenosis ≥70% confirmed by computed tomography angiography (CTA) or digital subtraction angiography (DSA)—ACS defined as proximal internal carotid artery (ICA) stenosis and aICAS as M1-segment middle cerebral artery stenosis, without concomitant vertebrobasilar involvement; (3) normal or corrected-to-normal vision; and (4) absence of transient ischemic attack or cerebral infarction within the preceding 6 months. Exclusion criteria were: (1) traumatic brain injury with residual neurological sequelae; (2) severe cognitive impairment precluding task completion; (3) psychiatric or other neurological disorders; and (4) concomitant severe cardiac, hepatic, or renal dysfunction. Control participants were matched by age, sex, and education level, with intracranial and extracranial stenosis excluded via neuroimaging. The study was conducted in accordance with the Declaration of Helsinki and approved by the Ethics Committee at the General Hospital of Central Theater Command (Wuhan, China) ([2024]008-01). All of the study's participants have signed informed consent forms.

2.2 Neuropsychological Assessments

Global cognitive function was evaluated using the Chinese version of the Mini-Mental State Examination, formally designated the Chinese Mini-Mental Status (CMMS) examination as revised and normed for the Chinese population by Katzman et al. [22], with a score <26 indicating impairment. Domain-specific cognition was assessed with the TMT Parts A and B (TMT-A/B). TMT-A evaluated visual search speed, sustained attention, and informa-

tion processing speed; TMT-B assessed executive function, cognitive flexibility, and task-switching ability. Completion time served as the primary outcome measure for both tests, with shorter durations reflecting better performance [23]. All neuropsychological assessments were completed before EEG recording and were administered by separate experimenters who were blinded to the participants' group assignments.

2.3 EEG Data Acquisition and Preprocessing

Continuous EEG was recorded using a 64-channel Ag/AgCl electrode cap and an eego™ 64 amplifier (E225, ANT Neuro Inc., Hengelo, Netherlands) at a sampling rate of 1000 Hz, with electrode impedances maintained below 10 kΩ. Resting-state data (5 min duration) were acquired under eyes-open conditions in a quiet, wakeful state.

Offline preprocessing was conducted in MATLAB R2022b (The MathWorks, Inc., Natick, MA, USA; https://www.mathworks.com/products/matlab.html) with EEGLAB 2021.0(Swartz Center for Computational Neuroscience, University of California San Diego, La Jolla, CA, USA; https://eeglab.org/): (1) non-neural channels removed, data re-referenced to common average; (2) band-pass filtering (0.5–40 Hz) and 50 Hz notch filtering; (3) segmentation into 2-s epochs; (4) independent component analysis-based removal of ocular and muscular artifacts, supplemented by manual rejection (±100 μV threshold); and (5) CPz (centroparietal midline electrode) restored, yielding 62 valid channels. For participants with right-side lesions and a matched CG subset, left-right hemispheric transposition standardized the affected hemisphere across groups.

2.4 Microstate Analysis

Microstate analysis was performed in Cartool software 3.9 (Functional Brain Mapping Laboratory, University of Geneva, Geneva, Switzerland; https://sites.google.com/site/cartoolcommunity/) within MATLAB R2022b [24], with an additional 2–20 Hz band-pass filter applied to suppress high-frequency noise and enhance topographic stability. Global Field Power (GFP) was computed as:

$$GFP = \sqrt{\frac{\sum_{i}^{N} \left(V_i(t) - V_{mean}(t)\right)^2}{N}}$$

where N is the total electrode count, V_i(t) is the voltage of channel i at time t, and V_mean(t) is the cross-channel mean voltage. Spatial topographies at GFP peaks were extracted and submitted to a modified k-means clustering algorithm, with map polarity ignored. Cross-validation identified 4 as the optimal cluster number, yielding 4 microstate templates corresponding to the canonical microstate classes A–D. These templates were back-fitted to each participant's preprocessed EEG, with each time sample assigned to the template showing the highest polarity-independent spatial correlation. Four temporal parameters were extracted per microstate class: mean duration (Dur), fractional coverage (Cov), occurrence rate (Occ), and inter-class transition probability (TP) [25].

2.5 Power Spectrum Analysis

Spectral power was computed via Fast Fourier Transform on the preprocessed data and decomposed into five canonical frequency bands: δ (1–4 Hz), θ (4–8 Hz), α (8–13 Hz), β (13–30 Hz), and γ (30–40 Hz). Whole-brain absolute power values were then compared statistically across the three groups of participants.

2.6 Functional Connectivity Analysis

To mitigate volume-conduction effects, source reconstruction was performed using the FieldTrip toolbox (Donders Institute for Brain, Cognition and Behaviour, Radboud University, Nijmegen, the Netherlands; https://www.fieldtriptoolbox.org/). Following the preprocessing and artifact correction procedures described in Section 2.3, artifact-free EEG epochs were re-referenced to the common average. The α-band activity (8–13 Hz) was estimated using a multitaper Fourier transform centered at 10.5 Hz with ± 2.5-Hz spectral smoothing. A standard three-shell boundary element model served as the forward solution, and a partial canonical correlation (PCC) beamformer with 10% regularization and fixed dipole orientation projected sensor-space signals into cortical source space. Time series from 76 regions of interest were subsequently extracted using the Automated Anatomical Labeling (AAL) atlas to construct an epoch-wise source activation model [26].

Functional connectivity (FC) was quantified using the Phase Locking Value (PLV), reflecting inter-regional phase synchronization:

$$PLV(t,f) = \frac{1}{N}\left|\sum_{n=1}^{N} e^{i(\phi_{n,x}(t,f)-\phi_{n,y}(t,f))}\right|$$

where t is time, f the target frequency band, n a specific epoch, N the total epoch count, and Φn,x and Φn,y the instantaneous phases of regions x and y in epoch n. PLV values range from 0 to 1, with higher values indicating stronger synchronization. A 76 × 76 PLV matrix was constructed in the α-band for each participant. The α-band was selected because it is the dominant resting-state EEG rhythm and is sensitive to alterations in cortical synchronization associated with cerebral ischemia and cognitive processing. Group differences were assessed using the Network-Based Statistic (NBS), with an initial edge-level threshold of $p < 0.01$ ($t = 2.684$). Component-level family-wise error correction was performed using 5000 permutations, with corrected $p < 0.05$ considered significant. NBS inference was made at the network-component level rather than for indi-

vidual connections [27]. FC networks were visualized with BrainNet Viewer 1.7 (Beijing Normal University, Beijing, China; https://www.nitrc.org/projects/bnv/) [28].

2.7 Statistical Analysis

Statistical analyses were performed in SPSS v27.0 (IBM Corp., Armonk, NY, USA), Python 3.12 (Python Software Foundation, Wilmington, DE, USA), and R 4.2.1 (R Foundation for Statistical Computing, Vienna, Austria). Distributional normality was assessed using the Shapiro–Wilk test and homogeneity of variance using Levene's test. Microstate parameters were analyzed using one-way ANOVA followed by Bonferroni-adjusted pairwise comparisons, or the Kruskal–Wallis test as appropriate. Omnibus ANOVA results are reported with partial η squared (ηp^2), and pairwise comparisons were reported with 95% confidence intervals where internally consistent estimates were available. Microstate–cognition associations were examined using partial Pearson correlations adjusted for age, hypertension, and diabetes; rank-based partial Spearman correlations were used as sensitivity analyses. Receiver operating characteristic (ROC) analyses were conducted separately for each selected microstate metric. Apparent area under the curve (AUC) 95% confidence intervals were estimated using 2000 stratified bootstrap samples. Internal validation used repeated stratified five-fold cross-validation (100 repetitions); the Youden threshold was selected within each training fold and evaluated only in its corresponding validation fold. AUC p values were false discovery rate (FDR)-adjusted separately within the ACS-vs.-CG and aICAS-vs.-CG indicator families. FC group differences were tested by independent-samples t-tests with NBS correction implemented in GRETNA 2.0.0 (State Key Laboratory of Cognitive Neuroscience and Learning, Beijing Normal University, Beijing, China; primary threshold $p < 0.01$, 5000 permutations; corrected $p < 0.05$) [29]. All tests were two-tailed, with significance set at $p < 0.05$.

3. Results

3.1 Demographic Characteristics

The demographic profiles and distribution of vascular risk factors for the three cohorts are summarized in Table 1. No significant differences were observed across the groups regarding baseline metrics, including age, sex, years of education, hypertension, diabetes, and history of smoking or alcohol consumption ($p > 0.05$), confirming baseline comparability across groups.

3.2 Neuropsychological Assessments

CMMS scores did not differ significantly among groups ($p = 0.122$). However, domain-specific cognitive assessments revealed significant group differences in the completion times for both TMT-A ($p = 0.004$) and TMT-B ($p = 0.010$). Post hoc comparisons demonstrated that only the ACS group required significantly more time on TMT-A ($p = 0.003$) and TMT-B ($p = 0.008$) tasks than did the CG group. No significant TMT differences were found between aICAS and controls (TMT-A: $p = 0.188$; TMT-B: $p = 0.377$) (Table 2).

3.3 rs-EEG Microstate Analysis

Using the k-means clustering algorithm, the rs-EEG data from the three cohorts were clustered into four distinct microstate classes, which aligned highly with the canonical maps reported in previous rs-EEG microstate studies (**Supplementary Fig. 1**). The mean duration of microstate A (MsA) exhibited significant group-level differences ($F(2,65) = 5.637$, $p = 0.006$, $\eta_p^2 = 0.15$). Post-hoc tests on the mean duration of MsA across the three groups revealed that the duration was significantly shorter in the ACS group than in the control group ($p = 0.004$; mean-difference 95% CI, 0.003–0.016), whereas no significant difference was observed in the aICAS group ($p = 0.241$; 95% CI, –0.002 to 0.013). For mean occurrence, the frequency of microstate B (MsB) also differed significantly among the groups ($F(2,65) = 3.343$, $p = 0.042$, $\eta_p^2 = 0.093$), showing a significant increase in the ACS group relative to CG ($p = 0.048$; 95% CI, –1.879 to –0.007), with no significant alteration in the aICAS group ($p = 1.0$; 95% CI, –1.269 to 0.823). Furthermore, the coverage of MsA showed a significant main effect of group ($F(2,65) = 6.007$, $p = 0.004$, $\eta_p^2 = 0.156$), characterized by a significant reduction in both the ACS ($p = 0.012$; 95% CI, 1.007–10.415) and aICAS ($p = 0.012$; 95% CI, 1.149–11.842) groups compared to the control group. Analysis of transition probabilities revealed that both the ACS ($p = 0.039$; 95% CI, 0.086–4.450) and aICAS ($p = 0.040$; 95% CI, 0.089–5.088) groups demonstrated a significantly decreased rate of transition between MsA and microstate C (MsC). Notably, as a cohort-specific feature, the aICAS group exhibited a significant increase in the bidirectional transition rate between MsB and microstate D (MsD) ($p = 0.025$; 95% CI, –3.026 to –0.155)—a distinct neurophysiological alteration that was not observed in the ACS cohort ($p = 0.111$; 95% CI, –2.339 to 0.168) (Fig. 1).

3.4 Correlations Between Microstate Parameters and Neuropsychological Assessments, and ROC Curve

After adjustment for age, hypertension, and diabetes, MsA duration was negatively correlated with TMT-B completion time in the ACS group (partial r = –0.420, 95% CI, –0.704 to –0.020, $p = 0.041$), but not with TMT-A ($p = 0.074$). MsA coverage was negatively correlated with TMT-A (partial r = –0.491, 95% CI, –0.756 to –0.087, $p = 0.020$), but not with TMT-B ($p = 0.062$). No significant associations were found between TMT performance and the MsA–MsC transition probability. In the aICAS group, the MsB-to-MsD transition probability was negatively correlated with both TMT-A (partial r = –0.636, 95% CI, –0.886 to –0.098, $p = 0.026$) and TMT-B completion times (partial

Table 1. Demographic characteristics of the participants.

Variable	CG (n = 22)	ACS (n = 29)	aICAS (n = 17)	F/χ^2	*p*	Follow-up analysis[a]
	Mean (SD)	Mean (SD)	Mean (SD)			
Age (years)	54.32 (7.18)	58.76 (7.33)	54.71 (8.21)	2.705	0.074	ns
Sex (female/male)	4/18	7/22	3/14	$\chi^2_{0.05,2} = 0.391$	0.822	NA
Hypertension	11	16	12	$\chi^2_{0.05,2} = 1.760$	0.415	NA
Diabetes	14	18	11	$\chi^2_{0.05,2} = 0.034$	0.983	NA
Smoking	10	15	3	$\chi^2_{0.05,2} = 5.384$	0.068	NA
Alcohol	8	8	2	$\chi^2_{0.05,2} = 3.014$	0.222	NA
Education (years)	8.45 (2.56)	10.03 (2.78)	9.71 (3.27)	2.028	0.140	ns

CG, control group; ACS, asymptomatic carotid stenosis; aICAS, asymptomatic intracranial atherosclerotic stenosis; SD, standard deviation; ns, not significant; NA, not applicable.

[a]Follow-up analysis based on Bonferroni correction.

Table 2. Psychological assessment of the participants.

Variable	CG (n = 22)	ACS (n = 29)	aICAS (n = 17)	F	*p*	Follow-up analysis[a]
	Mean (SD)	Mean (SD)	Mean (SD)			
TMT-A	56.00 (18.99)	74.62 (18.87)	67.65 (19.39)	6.004	0.004	0.003[b] 0.188[c]
TMT-B	52.23 (15.23)	68.38 (19.09)	61.35 (20.13)	4.920	0.010	0.008[b] 0.377[c]
CMMS	29.18 (0.59)	28.62 (1.15)	28.71 (1.11)	2.172	0.122	ns

CMMS, Chinese Mini-Mental Status; TMT-A, Trail Making Test A; TMT-B, Trail Making Test B.

[a]Follow-up analysis based on Bonferroni correction.

[b]*p*-value between ACS and CG in Bonferroni correction.

[c]*p*-value between aICAS and CG in Bonferroni correction.

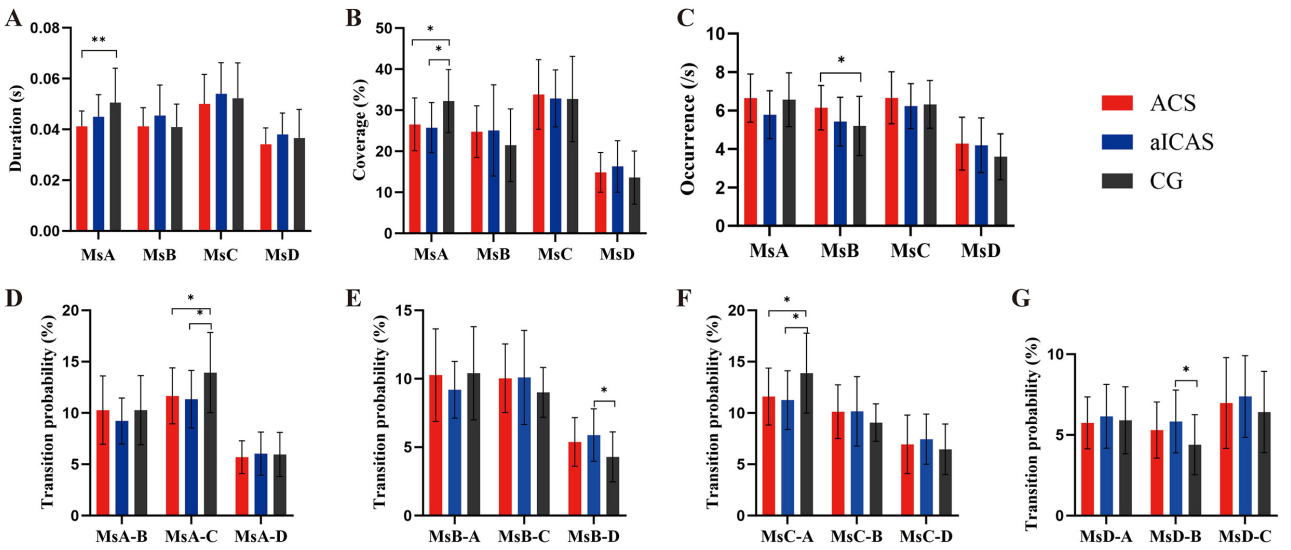


Fig. 1. Comparison of the basic parameters of microstates among the three groups. (A) Mean duration. (B) Coverage. (C) Mean occurrence. (D) Transition probability (TP) from microstate A to other microstate types. (E) TP from microstate B to other microstate types. (F) TP from microstate C to other microstate types. (G) TP from microstate D to other microstate types. *$p < 0.05$; **$p < 0.01$.

r = –0.592, 95% CI, –0.870 to –0.027, $p = 0.043$) (Fig. 2 and **Supplementary Table 1**).

ROC analyses showed moderate discrimination by individual microstate metrics. For ACS vs. CG, MsA duration yielded an AUC of 0.741 (95% CI, 0.597–0.863; cross-validated AUC = 0.744), and MsA coverage yielded an AUC of 0.732 (95% CI, 0.577–0.857; cross-validated AUC = 0.726). For aICAS vs. CG, MsA coverage yielded

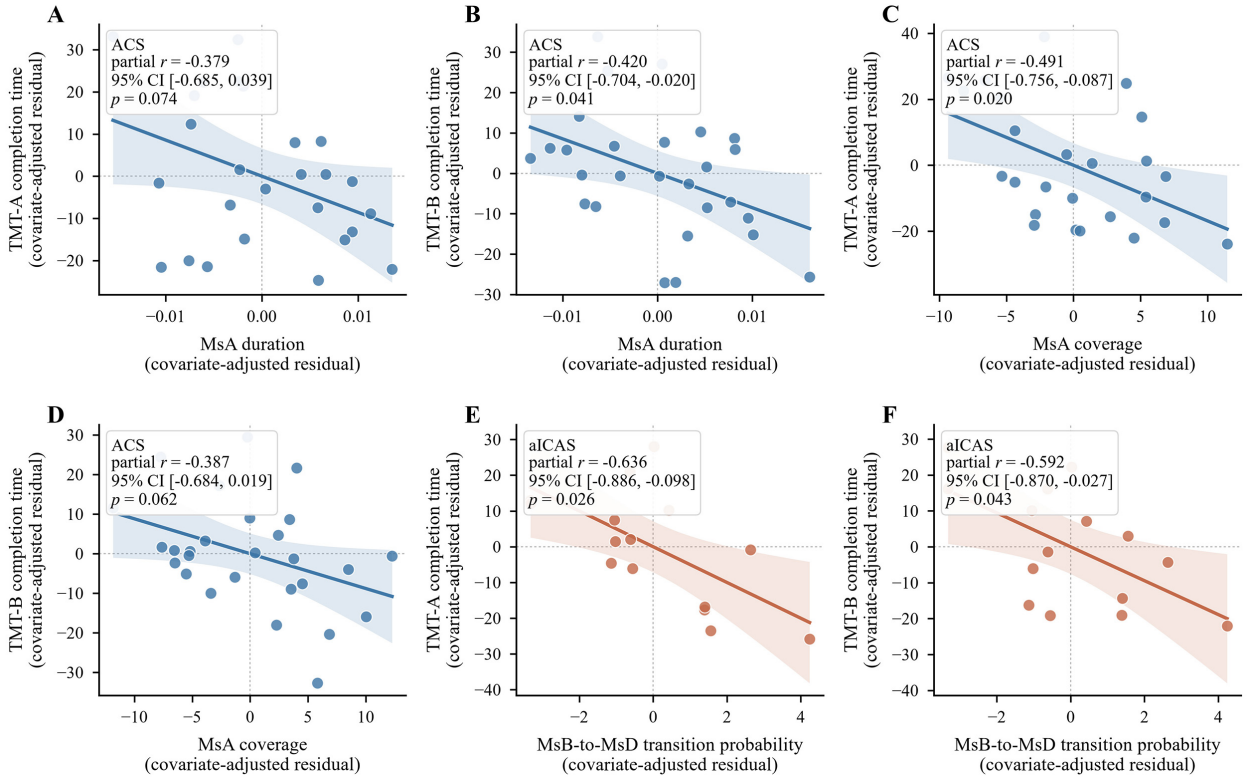


Fig. 2. Correlations between TMT-A and TMT-B completion times and key microstate parameters in the ACS and aICAS groups. (A,B) Correlations between TMT-A and TMT-B completion times and the mean duration of MsA in the ACS group. (C,D) Correlations between TMT-A and TMT-B completion times and MsA coverage in the ACS group. (E,F) Correlations between TMT-A and TMT-B completion times and the MsB–D transition probability in the aICAS group. MsA, microstate A.

an AUC of 0.744 (95% CI, 0.578–0.887; cross-validated AUC = 0.743), and the MsB-to-MsD transition probability yielded an AUC of 0.719 (95% CI, 0.545–0.865; cross-validated AUC = 0.720). Overall, AUCs ranged from 0.672 to 0.744 (Fig. 3). Optimal cut-offs, sensitivity, and specificity are reported in **Supplementary Table 2**. These internally validated results are exploratory because no independent external validation cohort was available.

3.5 Power Spectrum and α-Band Functional Connectivity Analyses

Power spectrum analysis demonstrated significantly lower α-band power among patients with ACS than among the CG group. For the source-space FC analysis, the ACS group exhibited significantly enhanced FC within the α-band (26 nodes and 36 unique undirected edges; NBS family-wise error-corrected $p = 0.04599$; primary edge-forming threshold $p < 0.01$, corresponding to $t = 2.684$). The edge-level t values within this component ranged from 2.684 to 4.139, corresponding to descriptive Cohen's d values of 0.759–1.170 (Fig. 4). No α-band FC component was significant for aICAS vs. CG after NBS correction (**Supplementary Fig. 2**).

The significant ACS–CG component comprised distributed frontal, occipital, temporal, insular, and cingulate connections, including 18 right intrahemispheric, 6 left intrahemispheric, and 12 interhemispheric edges. Prominent connections involved the bilateral parahippocampal gyri, the right insula and left anterior cingulate/paracingulate gyri, and the left medial superior frontal and right transverse temporal gyri. The left medial superior frontal gyrus and right insula were among the most frequently involved regions (Fig. 5). The complete list of connections and their descriptive edge-level statistics is provided in **Supplementary Table 3** (AAL76 atlas).

4. Discussion

Using rs-EEG microstate analysis, power spectrum analysis, and α-band PLV functional connectivity, the present study compared functional brain network architecture across ACS, aICAS, and control cohorts. Both stenosis groups showed reduced MsA coverage and decreased MsA–MsC transition efficiency. ACS was further characterized by shortened MsA duration, reduced α-band power, and distributed increases in intra- and interhemispheric α-band functional connectivity, presenting a pattern of concurrent power attenuation and hyperconnectivity that did not follow from stenosis severity alone. The aICAS group, by contrast, showed elevated MsB–MsD transition rates with no FC alterations surviving NBS correction. These

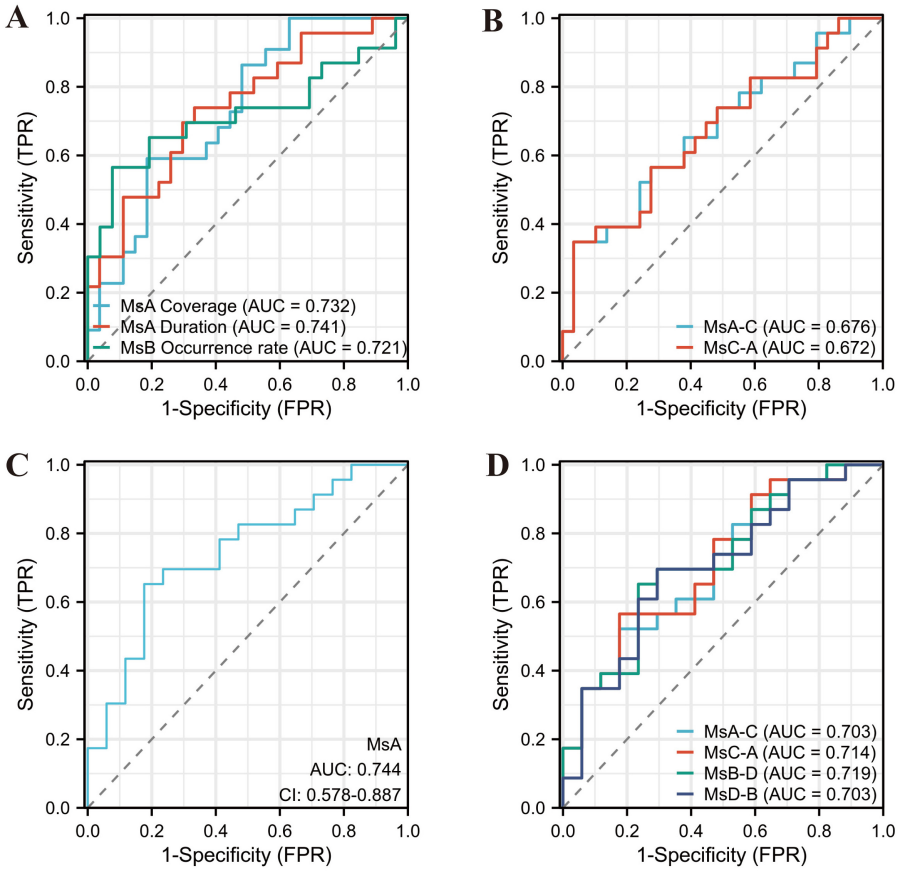


Fig. 3. ROC curves of basic microstate parameters for the asymptomatic stenosis group vs. the CG group. (A,B) Comparisons of ACS vs. the CG: MsA coverage AUC = 0.732, mean duration AUC = 0.741, mean occurrence AUC = 0.721, MsA-to-C transition rate AUC = 0.676, MsC-to-A transition rate AUC = 0.672. (C,D) Comparisons of aICAS vs. the CG: MsA coverage AUC = 0.744, MsA-to-C transition rate AUC = 0.703, MsC-to-A transition rate AUC = 0.714, MsB-to-D transition rate AUC = 0.719, MsD-to-B transition rate AUC = 0.703. ROC, receiver operating characteristic; AUC, area under the curve; TPR, true positive rate; FPR, false positive rate.

findings revealed distinct electrophysiological patterns associated with extracranial and intracranial atherosclerotic stenosis and suggested that stenosis location may have influenced the spatial and temporal characteristics of functional brain reorganization.

Both patient groups showed reduced MsA coverage and a decline in bidirectional transition rates between MsA and MsC. MsA has been associated with sensorimotor and auditory network activity, whereas MsC has been linked to the default-mode and saliency networks, which underlie attention regulation and inhibitory control [30]. The reduced transition rate therefore indicated declining dynamic integration between primary sensory processing and higher-order cognitive regulation, amounting to a functional sensory-saliency decoupling [31]. This shared deficit likely originated in thalamic compromise driven by chronic hypoperfusion, broadly disrupting state-switching across global brain networks [19,32]. Notably, MsA coverage was already significantly reduced in the aICAS group despite the absence of TMT differences from controls, suggesting that EEG microstate analysis may have captured early functional network alterations that are not yet detectable using conventional cognitive assessments [33].

At the cellular level, chronic cerebral hypoperfusion can produce an imbalance between energy supply and demand, impair ATP-dependent ion-pump function, and disturb synaptic glutamate homeostasis [34,35]. Those alterations can affect neuronal excitability and synchronization and may ultimately manifest as changes in oscillatory activity and microstate-transition dynamics. Despite comparable degrees of vascular stenosis, the ACS and aICAS groups exhibited different electrophysiological and cognitive profiles, suggesting that the location and hemodynamic consequences of stenosis may have shaped the pattern of functional brain reorganization [36]. Proximal ICA stenosis may have exerted broader effects on hemispheric perfusion, whereas M1-segment stenosis may have involved a more circumscribed vascular territory and greater heterogeneity in collateral support. Therefore, integrating electrophysiological measures with stenosis severity, collateral circulation, and cerebrovascular reserve may have provided a more comprehensive assessment of functional brain sta-

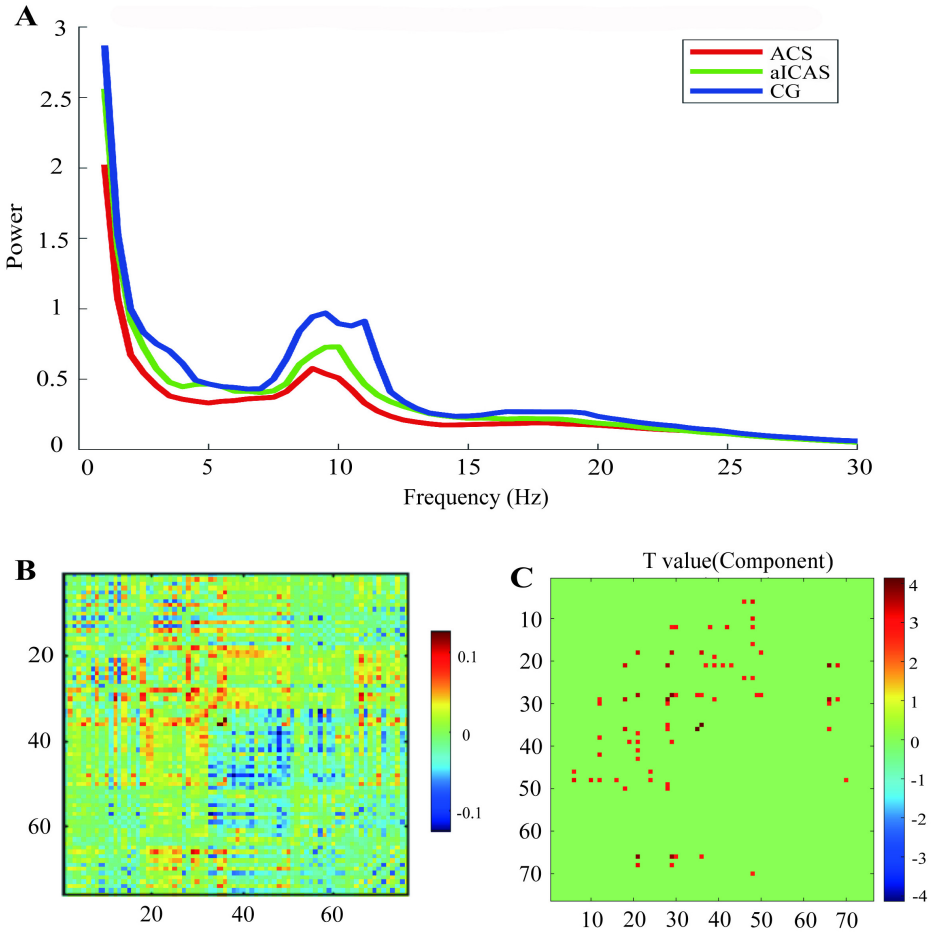


Fig. 4. Power spectra and α-band functional connectivity differences between the ACS and CG groups. (A) Power spectrum analysis results for the three subject groups, displayed over 1–30 Hz; spectral analysis covered the full 1–40 Hz range. (B) Adjacency matrix of differential connectivity for the ACS group relative to the CG. (C) Statistical t-value map of α-band phase-locking value (PLV) comparisons between ACS and CG, with red indicating enhanced functional connectivity in ACS.

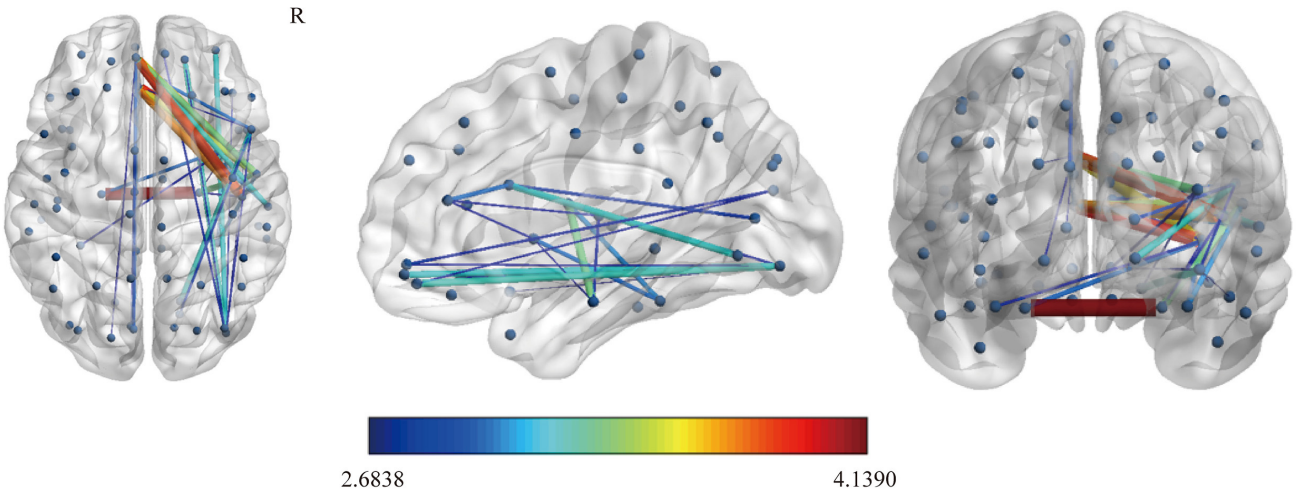


Fig. 5. The FC map highlights brain regions with significant differences between the ACS and CG groups. All connections shown are stronger in the ACS group, with more intense red representing a higher statistical significance. "R" denotes the right cerebral hemisphere.

IMR Press

tus and residual adaptive capacity than would anatomical stenosis severity assessment alone.

Beyond these shared features, the ACS group was specifically characterized by shortened MsA duration and increased MsB occurrence. Shortened MsA duration pointed to further instability of sensorimotor network activation, whereas increased MsB occurrence, linked to bilateral occipital visuospatial processing, likely reflected compensatory redistribution of sensory resources [37]. Elevated MsB occurrence has previously been associated with cognitive impairment severity in Alzheimer's disease and cerebral small vessel disease [38,39]; the present findings extended this observation to a subclinical ACS population. After adjustment for age, hypertension, and diabetes, shorter MsA duration was associated with longer TMT-B completion time, whereas lower MsA coverage was associated with longer TMT-A completion time. These associations suggested that reduced stability and engagement of MsA-related networks may contribute to slower information processing and executive performance in ACS. The corresponding associations between MsA duration and TMT-A and between MsA coverage and TMT-B were not statistically significant, indicating that different MsA parameters may relate to distinct aspects of TMT performance [40,41].

At the FC level, global α-band power in the ACS group was significantly lower than in controls, consistent with reduced neuronal metabolic efficiency and compromised thalamocortical oscillatory loops under sustained hypoperfusion [42]. In addition, α-band PLV FC showed widespread enhancement: anteroposterior prefrontal–occipital connections were upregulated ipsilateral to the stenosis; cross-hemispheric synchronization increased between the ipsilateral prefrontal lobe and the contralateral temporal lobe and bilateral parahippocampal gyri; and the contralateral insula showed broadly enhanced connectivity with bilateral anterior cingulate, parahippocampal, and fusiform regions [43]. This combination of power attenuation and connectivity enhancement may have reflected a potentially compensatory hyperconnectivity pattern in which increased remote phase synchronization helped maintain global communication when local spontaneous oscillatory activity was weakened. The prominent role of the contralateral insula in this reorganization suggested that the unaffected hemisphere may have participated in cross-network remodeling [44,45]. Taken together, ACS presents a pattern of neural reorganization that may be associated with the widespread, sustained hypoperfusion characteristic of proximal ICA stenosis, in which enhanced network-level coherence may partly compensate for reduced local oscillatory efficiency under progressive ischemic constraint.

The aICAS-specific findings centered on a significant bidirectional increase in MsB–MsD transition rates. MsD corresponds to the dorsal attention network, governing executive control within frontoparietal regions [46]. The heightened visual-to-attention network transitioning may have reflected adaptive reorganization after intracranial stenosis-induced disruption of long-range cortical connections. After adjustment for age, hypertension, and diabetes, TMT completion times correlated negatively with MsB–MsD transition rates, suggesting that this topological shift may have potential compensatory relevance at the current subclinical stage, consistent with the increased P300 amplitudes previously reported by our group in aICAS patients as a marker of compensatory attentional recruitment [47]. This specific pattern may have been influenced by the vascular anatomy of intracranial stenosis: the affected territory is typically more circumscribed and often benefits from retrograde hemodynamic support via leptomeningeal collaterals [48]. Under those conditions, intermittent perfusion fluctuations may promote adaptive reorganization at the level of specific network state-switching, rather than the sustained single-network instability seen in ACS, potentially representing a temporally concentrated strategy suited to the more localized ischemic territory.

No significant α-band FC differences were found between the aICAS and control groups after NBS correction. This absence may have been related to two complementary factors: the circumscribed ischemic territory may have received collateral support, reducing the extent of global phase-synchronous reorganization; and functional alterations in aICAS may have been more prominently expressed through microstate transitioning, a short-timescale mechanism that may not produce detectable changes in large-scale PLV network organization. This contrasted fundamentally with the pervasive hypoperfusion driving ACS reorganization [3]. The differing FC profiles thus further validated the location-specific pathophysiology separating the two stenosis subtypes. Global spatial hyperconnectivity in ACS and altered temporal switching in aICAS may have represented different electrophysiological responses to lesions that differed in vascular territory, chronicity, and collateral capacity, suggesting that these EEG alterations may have reflected both disease-related disruption and potentially adaptive reorganization under sustained ischemic constraint.

These divergent EEG profiles indicated how topographical specificity may have shaped functional network remodeling. The enhanced functional connectivity observed in ACS may have provided candidate electrophysiological features for monitoring network changes associated with revascularization, consistent with previous evidence that EEG FC may normalize after successful revascularization. In contrast, the altered microstate switching observed in aICAS may provide a potential target for future studies of network-level modulation. ROC analyses yielded AUC values of 0.672–0.744 for individual metrics, indicating moderate discriminatory performance, with comparable results obtained through repeated five-fold cross-validation. However, because no independent external validation co-

hort was available, these indicators should be regarded as exploratory candidate markers rather than established clinical biomarkers.

5. Limitations

Several limitations should be acknowledged. First, the sample size, particularly in the aICAS group (n = 17), was relatively modest. Although a priori power analysis was performed, the large number of electrophysiological parameters increased the risk of false-positive findings. Therefore, the results require validation in larger, multi-center cohorts. Second, the cross-sectional design precluded causal inference. The observed alterations may have partly reflected adaptive or compensatory responses, but disease-related disruption cannot be excluded. Third, the absence of concurrent perfusion imaging prevented direct assessment of collateral circulation, cerebrovascular reserve, cerebral perfusion, and their relationships with EEG alterations. Fourth, despite source reconstruction, PLV estimates may have remained affected by residual spatial leakage, and the FC analysis was limited to the α-band. Finally, TMT and CMMS may not have captured subtle domain-specific cognitive changes. The ROC analyses used internal cross-validation but lacked an independent external cohort; therefore, the performance estimates and cut-offs remained exploratory and sample-dependent. Larger longitudinal studies incorporating perfusion imaging, comprehensive cognitive assessment, broader frequency bands, and external validation are needed.

6. Conclusions

The present study identified distinct subclinical patterns of functional brain reorganization in ACS and aICAS through rs-EEG analysis spanning microstate dynamics, power spectra, and functional connectivity, and suggested that stenosis location may be associated with different electrophysiological profiles. These findings supported the potential value of rs-EEG metrics for characterizing functional brain alterations in asymptomatic cerebrovascular disease. However, the observed EEG changes should be interpreted as possible functional reorganization rather than direct evidence of compensatory neuroplasticity. Given the cross-sectional design, limited sample size, and moderate internally validated discriminative performance, larger longitudinal studies with independent external validation are required.

Availability of Data and Materials

Data available on request due to privacy/ethical restrictions.

Author Contributions

Conceptualization: JS, GX; Methodology: PZ, XS; Formal analysis and investigation: PZ, HL; Writing – original draft preparation: PZ, XS, HL; Writing – review and editing: XS, HZ, KL, ZL, JS; Funding acquisition: JS; Data acquisition: PZ, HL, HZ, KL, ZL; Resources: HZ, KL, ZL; Supervision: JS, GX. All authors contributed to editorial changes in the manuscript. All authors read and approved the final version of the manuscript. All authors have participated sufficiently in the work and agreed to be accountable for all aspects of the work.

Ethics Approval and Consent to Participate

The study was conducted in accordance with the Declaration of Helsinki and approved by the Ethics Committee at the General Hospital of Central Theater Command (Wuhan, China) ([2024]008-01). All of the study's participants have signed informed consent forms. The study was reported in accordance with the Strengthening the Reporting of Observational Studies in Epidemiology (STROBE) guidelines.

Acknowledgment

We acknowledge the participation and support of the patients and families in this study.

Funding

This work was supported by the Wuhan Key Research and Development Program (Grant No. 2025061202030422) and Hubei Provincial Clinical Medical Research Center for Minimally Invasive Treatment of Cerebrovascular Diseases.

Conflicts of Interest

The authors declare no conflicts of interest.

Supplementary Material

Supplementary material associated with this article can be found, in the online version, at https://doi.org/10.31083/JIN55171.

References

[1] GBD 2021 Stroke Risk Factor Collaborators. Global, regional, and national burden of stroke and its risk factors, 1990-2021: a systematic analysis for the Global Burden of Disease Study 2021. The Lancet. Neurology. 2024; 23: 973–1003. https://doi.org/10.1016/S1474-4422(24)00369-7

[2] de Weerd M, Greving JP, Hedblad B, Lorenz MW, Mathiesen EB, O'Leary DH, et al. Prevalence of asymptomatic carotid artery stenosis in the general population: an individual participant data meta-analysis. Stroke. 2010; 41: 1294–1297. https://doi.org/10.1161/STROKEAHA.110.581058

[3] Gutierrez J, Turan TN, Hoh BL, Chimowitz MI. Intracranial atherosclerotic stenosis: risk factors, diagnosis, and treatment. The Lancet. Neurology. 2022; 21: 355–368. https://doi.org/10.1016/S1474-4422(21)00376-8

[4] Liu Y, Zou Y, Zhou H, Ding M, Liu N, Guo H, et al. Prognosis of incidentally detected asymptomatic intracranial atherosclerotic stenosis: A prospective hospital-based cohort study. International Journal of Stroke: Official Journal of the Interna-

tional Stroke Society. 2026; 21: 625–634. https://doi.org/10.1177/17474930251383855

[5] Endara-Mina J, Escudero CJ, Carreño K, Intriago C, López-Carrera R. Carotid Stenosis and Cognitive Function: An Update on Therapeutic Interventions. Cureus. 2025; 17: e81908. https://doi.org/10.7759/cureus.81908

[6] Krebs JR, Anderson EM, Fazzone B, Agaba P, Shah SK. Asymptomatic Carotid Artery Stenosis, Cognitive Function, and the Impact of Carotid Revascularization: A Narrative Review. Annals of Vascular Surgery. 2025; 113: 298–304. https://doi.org/10.1016/j.avsg.2024.06.048

[7] Liu T, Wang Y, Zhang K, Fan H, Li X, Wu X, et al. Evaluation of intracranial atherosclerotic stenosis burden, the use of dual antiplatelet therapy, and stroke recurrence in patients with minor stroke. Journal of Thrombosis and Haemostasis: JTH. 2025; 23: 2913–2925. https://doi.org/10.1016/j.jtha.2025.04.034

[8] Balestrini S, Lupidi F, Balucani C, Altamura C, Vernieri F, Provinciali L, et al. One-year progression of moderate asymptomatic carotid stenosis predicts the risk of vascular events. Stroke. 2013; 44: 792–794. https://doi.org/10.1161/STROKEAHA.112.671461

[9] Zhao Y, Gong CX. From chronic cerebral hypoperfusion to Alzheimer-like brain pathology and neurodegeneration. Cellular and Molecular Neurobiology. 2015; 35: 101–110. https://doi.org/10.1007/s10571-014-0127-9

[10] Zheng J, Peng S, Cui L, Liu X, Li T, Zhao Z, et al. Enriched environment attenuates hippocampal theta and gamma rhythms dysfunction in chronic cerebral hypoperfusion via improving imbalanced neural afferent levels. Frontiers in Cellular Neuroscience. 2023; 17: 985246. https://doi.org/10.3389/fncel.2023.985246

[11] Cui L, Hong H, Wang S, Zeng Q, Jiaerken Y, Yu X, et al. Small vessel disease and cognitive reserve oppositely modulate global network redundancy and cognitive function: A study in middle-to-old aged community participants. Human Brain Mapping. 2024; 45: e26634. https://doi.org/10.1002/hbm.26634

[12] Gao HL, Han BS, Zhang K, Wang ZL, Gao BL, Li TX, et al. Effects of carotid artery stenting on cognitive impairment in patients with severe symptomatic carotid artery stenosis. Medicine. 2022; 101: e30605. https://doi.org/10.1097/MD.0000000000030605

[13] Václavík D, Pakizer D, Hrbáč T, Roubec M, Procházka V, Jonszta T, et al. Changes in Cognitive Functions after Carotid Endarterectomy and Carotid Stenting: A Decade-Apart Comparison. Biomedicines. 2023; 12: 13. https://doi.org/10.3390/biomedicines12010013

[14] Galasko D, Abramson I, Corey-Bloom J, Thal LJ. Repeated exposure to the Mini-Mental State Examination and the Information-Memory-Concentration Test results in a practice effect in Alzheimer's disease. Neurology. 1993; 43: 1559–1563. https://doi.org/10.1212/WNL.43.8.1559

[15] Torkpoor R, Frolich K, Londos E, Nielsen TR. Diagnostic accuracy of the Swedish version of the multicultural cognitive examination for cognitive assessment in Swedish memory clinics. Journal of Alzheimer's Disease. 2024; 97: 715–726. https://doi.org/10.3233/JAD-230998

[16] Xue W, Qin Z, Zhong X, An L, Shi H, Wang H, et al. Altered frequency architecture of spontaneous brain activity in asymptomatic carotid stenosis: a wavelet-based resting-state fMRI study. Frontiers in Neurology. 2026; 17: 1683526. https://doi.org/10.3389/fneur.2026.1683526

[17] Quandt F, Fischer F, Schröder J, Heinze M, Kessner SS, Malherbe C, et al. Normalization of reduced functional connectivity after revascularization of asymptomatic carotid stenosis. Journal of Cerebral Blood Flow and Metabolism: Official Journal of the International Society of Cerebral Blood Flow and Metabolism. 2020; 40: 1838–1848. https://doi.org/10.1177/0271678X19874338

[18] Acharya D, Ruesch A, Schmitt S, Yang J, Smith MA, Kainerstorfer JM. Changes in neurovascular coupling with cerebral perfusion pressure indicate a link to cerebral autoregulation. Journal of Cerebral Blood Flow and Metabolism: Official Journal of the International Society of Cerebral Blood Flow and Metabolism. 2022; 42: 1247–1258. https://doi.org/10.1177/0271678X221076566

[19] Hsiao FJ, Hsieh FY, Chen WT, Chu DC, Lin YY. Altered Resting-State Cortical EEG Oscillations in Patients With Severe Asymptomatic Carotid Stenosis. Clinical EEG and Neuroscience. 2016; 47: 142–149. https://doi.org/10.1177/1550059414560396

[20] Lu HY, Ma ZZ, Zhang JP, Wu JJ, Zheng MX, Hua XY, et al. Altered Resting-State Electroencephalogram Microstate Characteristics in Stroke Patients. Journal of Integrative Neuroscience. 2024; 23: 176. https://doi.org/10.31083/j.jin2309176

[21] Faul F, Erdfelder E, Lang AG, Buchner A. G*Power 3: A flexible statistical power analysis program for the social, behavioral, and biomedical sciences. Behavior Research Methods. 2007; 39: 175–191. https://doi.org/10.3758/BF03193146

[22] Katzman R, Zhang MY, Ouang-Ya-Qu, Wang ZY, Liu WT, Yu E, et al. A Chinese version of the Mini-Mental State Examination; impact of illiteracy in a Shanghai dementia survey. Journal of Clinical Epidemiology. 1988; 41: 971–978. https://doi.org/10.1016/0895-4356(88)90034-0

[23] Bowie CR, Harvey PD. Administration and interpretation of the Trail Making Test. Nature Protocols. 2006; 1: 2277–2281. https://doi.org/10.1038/nprot.2006.390

[24] Brunet D, Murray MM, Michel CM. Spatiotemporal analysis of multichannel EEG: CARTOOL. Computational Intelligence and Neuroscience. 2011; 2011: 813870. https://doi.org/10.1155/2011/813870

[25] Li S, Hu R, Yan H, Chu L, Qiu Y, Gao Y, et al. Neurophysiological Markers of Auditory Verbal Hallucinations in Patients with Schizophrenia: An EEG Microstates Study. Brain Topography. 2025; 38: 29. https://doi.org/10.1007/s10548-025-01105-2

[26] Oostenveld R, Fries P, Maris E, Schoffelen JM. FieldTrip: Open source software for advanced analysis of MEG, EEG, and invasive electrophysiological data. Computational Intelligence and Neuroscience. 2011; 2011: 156869. https://doi.org/10.1155/2011/156869

[27] Lian J, Xu L, Song T, Peng Z, Zhang Z, An X, et al. Reduced Resting-State EEG Power Spectra and Functional Connectivity after 24 and 36 Hours of Sleep Deprivation. Brain Sciences. 2023; 13: 949. https://doi.org/10.3390/brainsci13060949

[28] Xia M, Wang J, He Y. BrainNet Viewer: a network visualization tool for human brain connectomics. PloS One. 2013; 8: e68910. https://doi.org/10.1371/journal.pone.0068910

[29] Zalesky A, Fornito A, Bullmore ET. Network-based statistic: identifying differences in brain networks. NeuroImage. 2010; 53: 1197–1207. https://doi.org/10.1016/j.neuroimage.2010.06.041

[30] Tarailis P, Koenig T, Michel CM, Griškova-Bulanova I. The Functional Aspects of Resting EEG Microstates: A Systematic Review. Brain Topography. 2024; 37: 181–217. https://doi.org/10.1007/s10548-023-00958-9

[31] Zhang Z, Li H, Huang Y, He Y, Xu W, Wu J, et al. EEG microstate dynamics reveal progressive sensorimotor network dysfunction across levels of anxiety severity in drug-naïve major depressive disorder. Journal of Affective Disorders. 2026; 402: 121373. https://doi.org/10.1016/j.jad.2026.121373

[32] Shine JM, Lewis LD, Garrett DD, Hwang K. The impact of the human thalamus on brain-wide information processing. Nature Reviews. Neuroscience. 2023; 24: 416–430. https://doi.org/10.1038/s41583-023-00701-0

[33] Tanaka M, Yamada E, Mori F. Neurophysiological markers of early cognitive decline in older adults: a mini-review of electroencephalography studies for precursors of dementia. Frontiers in Aging Neuroscience. 2024; 16: 1486481. https://doi.org/10.3389/fnagi.2024.1486481

[34] Rajeev V, Chai YL, Poh L, Selvaraji S, Fann DY, Jo DG, et al. Chronic cerebral hypoperfusion: a critical feature in unravelling the etiology of vascular cognitive impairment. Acta Neuropathologica Communications. 2023; 11: 93. https://doi.org/10.1186/s40478-023-01590-1

[35] Tukacs V, Mittli D, Györffy BA, Hunyady-Gulyás É, Hlatky D, Tóth V, et al. Chronic stepwise cerebral hypoperfusion differentially induces synaptic proteome changes in the frontal cortex, occipital cortex, and hippocampus in rats. Scientific Reports. 2020; 10: 15999. https://doi.org/10.1038/s41598-020-72868-w

[36] Ren J, Xu D, Mei H, Zhong X, Yu M, Ma J, et al. Asymptomatic carotid stenosis is associated with both edge and network reconfigurations identified by single-subject cortical thickness networks. Frontiers in Aging Neuroscience. 2023; 14: 1091829. https://doi.org/10.3389/fnagi.2022.1091829

[37] Liu Z, Xie T, Ma N. Resting-State EEG Microstates Dynamics Associated with Interindividual Vulnerability to Sleep Deprivation. Nature and Science of Sleep. 2024; 16: 1937–1948. https://doi.org/10.2147/NSS.S485412

[38] Jin X, Zhou Y, Zhang D, Chen X, Ruan J, Fang D. Analysis of brain dynamics changes in patients with cerebral small vessel disease-related cognitive impairment based on electroencephalogram microstates. European Journal of Medical Research. 2025; 30: 785. https://doi.org/10.1186/s40001-025-03037-w

[39] Lian H, Li Y, Li Y. Altered EEG microstate dynamics in mild cognitive impairment and Alzheimer's disease. Clinical Neurophysiology: Official Journal of the International Federation of Clinical Neurophysiology. 2021; 132: 2861–2869. https://doi.org/10.1016/j.clinph.2021.08.015

[40] Kim H, Teghipco A, Rorden C, Fridriksson J, Chaves M, Hillis AE. Hypoperfusion regions linked to National Institutes of Health Stroke Scale scores in acute stroke. NeuroImage. Clinical. 2025; 45: 103761. https://doi.org/10.1016/j.nicl.2025.103761

[41] Paraskevas KI, Mikhailidis DP, Spinelli F, Faggioli G, Saba L, Silvestrini M, et al. Asymptomatic carotid stenosis and cognitive impairment. The Journal of Cardiovascular Surgery. 2023; 64: 167–173. https://doi.org/10.23736/S0021-9509.23.12620-6

[42] De Ridder D, Vanneste S. Thalamocortical dysrhythmia and reward deficiency syndrome as uncertainty disorders. Neuroscience. 2024; 563: 20–32. https://doi.org/10.1016/j.neuroscience.2024.11.002

[43] Scheeringa R, Petersson KM, Kleinschmidt A, Jensen O, Bastiaansen MCM. EEG α power modulation of fMRI resting-state connectivity. Brain Connectivity. 2012; 2: 254–264. https://doi.org/10.1089/brain.2012.0088

[44] Fang S, Zhou C, Wang Y, Jiang T. Contralesional functional network reorganization of the insular cortex in diffuse low-grade glioma patients. Scientific Reports. 2021; 11: 623. https://doi.org/10.1038/s41598-020-79845-3

[45] Cargnelutti E, Maieron M, D'Agostini S, Ius T, Skrap M, Tomasino B. Exploring cognitive Landscapes: Longitudinal Dynamics of left insula gliomas using neuropsychological inquiry, fMRI, and intra-resection real time neuropsychological testing. NeuroImage. Clinical. 2024; 44: 103689. https://doi.org/10.1016/j.nicl.2024.103689

[46] Pei G, Hu M, He Y, Yang X, Liu H, Jiang B, et al. Disruption of low-frequency narrowband EEG microstate networks in Parkinson's disease with mild cognitive impairment. Journal of Neuroengineering and Rehabilitation. 2025; 22: 218. https://doi.org/10.1186/s12984-025-01747-0

[47] Li H, Wu F, Rong Z, Zhao P, Song J, Xu G. Differences in Cognitive Impairment and Functional Plasticity Between Asymptomatic Cerebral Arterial Stenosis and Asymptomatic Intracranial Atherosclerotic Stenosis: An Event-Related Potential Study. Journal of Integrative Neuroscience. 2025; 24: 46257. https://doi.org/10.31083/JIN46257

[48] Yang D, Cherian L, Arfanakis K, Schneider JA, Aggarwal NT, Gutierrez J. Intracranial atherosclerotic disease and neurodegeneration: a narrative review and plausible mechanisms. Journal of Stroke and Cerebrovascular Diseases: the Official Journal of National Stroke Association. 2024; 33: 108015. https://doi.org/10.1016/j.jstrokecerebrovasdis.2024.108015